

Comparative Study of Three-Dimensional Wing Drag Minimization by Different Optimization Techniques

Boris Epstein*

Academic College of Tel-Aviv-Yaffo, 61083 Tel Aviv, Israel

Antony Jameson†

Stanford University, Stanford, California 94305

Sergey Peigin‡

Israel Aerospace Industries, 70100 Lod, Israel

and

Dino Roman,§ Neal Harrison,¶ and John Vassberg**

The Boeing Company, Huntington Beach, California 92647

DOI: 10.2514/1.38216

The main goal of this paper is to document a comparative study of different computational-fluid-dynamics-based optimization techniques applied to the solution of a three-dimensional wing drag minimization problem. To achieve this objective, three optimization tools were used: SYN107 (Intelligent Aerodynamics International), MDOPT (The Boeing Company), and OPTIMAS (Israel Aerospace Industries). The first tool employs gradient-based search techniques using the continuous adjoint equation, the second one is a response-surface method, and the last one uses a floating-point genetic algorithm as its search engine. As the starting geometry, the public domain DPW-W1 wing (a test case for the Third AIAA Drag Prediction Workshop) was used. The comparisons included herein are provided in three stages: cross analysis of the initial geometry by the computational fluid dynamics tools employed in the optimizations, optimization of the initial geometry to minimum drag, and cross analysis of optimal shapes achieved by the optimization tools using all computational fluid dynamics tools employed. The cross analysis also includes results from an independent computational fluid dynamics method that was not used in any of the optimization efforts. These results help quantify the level of variation that is inherent in, and can be expected from, application of the current state-of-the-art aerodynamic optimization methods. The present work may be regarded as a move toward the construction of reliable test cases for an aerodynamic shape optimization problem. Another goal of this collaborative investigation is to collect lessons learned from this pilot project to help develop a model for an aerodynamic optimization workshop.

Nomenclature

C_D	=	total drag coefficient
C_L	=	total lift coefficient
C_M	=	total pitching moment coefficient
C_p	=	pressure coefficient
M	=	freestream Mach number
R/c	=	relative radius of the airfoil leading edge
Re	=	freestream Reynolds number
t/c	=	relative thickness of airfoil
N_{ws}	=	number of sectional airfoils
α	=	angle of attack
θ	=	trailing-edge angle of airfoil

I. Introduction

IN THE development of commercial aircraft, aerodynamic design plays a leading role during the preliminary design stage in which the external aerodynamic shape is typically finalized. This phase is estimated to cost \$60–120 million [1]. The final design would be normally carried out only upon the commercially promising completion of the preliminary stage. Hence, the preliminary design stage is crucial for the overall success of the project.

To additionally underline the importance of drag minimization, consider the task of delivering a payload between distant destinations. Based on the Breguet range equation, which applies to long-range missions of transport-type jet aircraft, the operator would have to reduce the payload (and thus the revenue) by 7.6% to recover a 1.0% increase in drag (see [1]). Because most airlines operate on small margins, this would most likely no longer be a profit-generating venture. This example illustrates that a 1% delta in total drag is a significant change.

That is why computational fluid dynamics (CFD)-driven aerodynamic shape design has aroused steadily increasing interest [2–11]. Along with improvement in the accuracy of CFD, its contribution to aerodynamic design steadily grows. In fact, the past three decades have brought a revolution in the entire process of aerodynamic design, due to the increasing role of computational simulation.

Early on, the applicability of CFD to aerodynamic design was confined to flow analysis in a limited range of flight conditions and aerodynamic shapes. Additional limitations were due to the variable levels of accuracy in the prediction of different aerodynamic characteristics. For example, accurate CFD estimation of sensitive flow characteristics such as drag and pitching moment of three-dimensional wings became available only in recent years when Navier–Stokes methods reached an acceptable level of maturity,

Presented as Paper 0326 at the 46th AIAA Aerospace Sciences Meeting and Exhibit, Reno, NV, 7–10 January 2008; received 23 April 2008; revision received 5 November 2008; accepted for publication 6 November 2008. Copyright © 2008 by B. Epstein, A. Jameson, S. Peigin, D. Roman, N. Harrison, and J. Vassberg. Published by the American Institute of Aeronautics and Astronautics, Inc., with permission. Copies of this paper may be made for personal or internal use, on condition that the copier pay the \$10.00 per-copy fee to the Copyright Clearance Center, Inc., 222 Rosewood Drive, Danvers, MA 01923; include the code 0021-8669/09 \$10.00 in correspondence with the CCC.

*Professor. Senior Member AIAA.

†Thomas V. Jones Professor of Engineering. Fellow AIAA.

‡Professor. Associate Fellow AIAA.

§Associate Technical Fellow. Senior Member AIAA.

¶Engineer. Member AIAA.

**Boeing Technical Fellow. Associate Fellow AIAA.

whereas reasonably accurate estimates of $\partial C_L / \partial \alpha$ were attainable in the middle of the 1970s using linear panel methods.

At the present time, the maturity of CFD solvers for accurate drag estimation and the efficiency level of search engines enables an attempt at the aerodynamic optimization problem in an engineering environment. With this end in view, CFD-based aerodynamic optimizers must be verified by means of reliable test cases. This verification presents a complicated problem because it is impractical to test every optimal shape in a wind tunnel.

In this connection, the main goal of this paper is to perform a comparative study of several different CFD-based optimization techniques applied to the solution of a 3-D wing drag minimization problem. Specifically, three optimization tools were used: SYN107, MDOPT, and OPTIMAS. Additionally, the authors desired to better understand the pros and cons of three very different approaches to aerodynamic shape optimization.

This paper presents the attempt to systematically cross analyze optimizations performed by different optimization tools in all three stages of the optimization process: CFD cross analysis of the initial geometry (performed by the CFD tools employed in optimization), multiple optimization by three different optimizers, and CFD cross analysis of the independently generated optimal shapes. The cross-analysis phase included application of the three CFD solvers employed in the optimizations, as well as one solver that was not used during any of the optimization efforts.

II. Statement of the Problem

The objective of the general multipoint optimization problem is to minimize the weighted combination C_D^{wtd} of drag coefficients at the main design and secondary design points (flight conditions):

$$C_D^{\text{wtd}} = \sum_{k=1}^K w_k C_D(k) \quad (1)$$

where K is the total number of the design points.

The solution is sought in the class of wing shapes subject to the following classes of constraints:

1) Aerodynamic constraints such as prescribed constant total lift coefficient $C_L^*(k)$ and minimum allowed pitching moment $C_M^*(k)$:

$$C_L(k) = C_L^*(k), \quad C_M(k) \geq C_M^*(k) \quad (2)$$

2) Geometric constraints on the shape of the wing surface in terms of properties of sectional airfoils at the prescribed wing span locations of relative thickness $(t/c)_i$, relative local thickness $(\Delta y/c)_{ij}$ at the given chord locations $(x/c)_{ij}$ (beam constraints), relative radius of leading edge $(R/c)_i$, and trailing-edge angle θ_i :

$$\begin{aligned} (t/c)_i &\geq (t/c)_i^*, & (\Delta y/c)_{ij} &\geq (\Delta y/c)_{ij}^*, & (R/c)_i &\geq (R/c)_i^* \\ \theta_i &\geq \theta_i^* \end{aligned} \quad (3)$$

where $i = 1, \dots, N_{\text{ws}}$ [N_{ws} is the total number of sectional airfoils subject to optimization]; $j = 1, \dots, N_{\text{bc}}(i)$ [$N_{\text{bc}}(i)$ is the total number of beam constraints at section i]; and values $(t/c)_i^*$, $(\Delta y/c)_{ij}^*$, θ_i^* , $(R/c)_i^*$, C_L^* , and C_M^* are prescribed parameters of the problem.

III. Test-Case Description

A. Initial Geometry

The public domain DPW-W1 wing from DPW-III (see [12]) was used as the initial geometry for the aerodynamic optimizations. Reference quantities for this wing are $S_{\text{ref}} = 290.322 \text{ mm}^2$, $C_{\text{ref}} = 197.556 \text{ mm}$, $X_{\text{ref}} = 154.245 \text{ mm}$ (relative to the wing root leading edge), and a semispan value of $b/2 = 762 \text{ mm}$. During the optimizations, the wing planform was fixed.

B. Design Points

1) The main design points are $M = 0.76$, $C_L = 0.5$, and $Re = 5 \times 10^6$.

2) The high Mach secondary design points are $M = 0.78$, $C_L = 0.5$, and $Re = 5 \times 10^6$.

3) The takeoff secondary design points are $M = 0.20$ and

$$C_L^{\text{max}}(\text{optimal}) \geq C_L^{\text{max}}(\text{original})$$

The selected design points at high Mach numbers are typical for transonic cruise flight conditions. The additional reason for this choice was that the first condition is the design point of the DPW-W1 wing in the framework of DPW-III.

C. Geometrical Constraints (Per Wing Design Section)

1) The geometrical constraints are $(t/c)_i \geq (t/c)_i^*$, where $(t/c)_i^*$ [for $i = 1$ (root), 2 (crank), 3 (tip)] is the maximum thickness for the original wing defining sections, and

$$(t/c)_1^* = (t/c)_2^* = (t/c)_3^* = 13.5\%$$

2) The thickness value of the original wing section at fixed x/c locations is

$$(t/c)_{ij}(x/c)_{ij} \geq (t/c)_{ij}^*(x/c)_{ij}$$

where $(t/c)_{ij}^*(x/c)_{ij}$. Beam constraints are

$$(x/c)_{11} = (x/c)_{21} = (x/c)_{31} = 0.20$$

$$(t/c)_{11}^* = (t/c)_{21}^* = (t/c)_{31}^* = 12.0\%$$

$$(x/c)_{12} = (x/c)_{22} = (x/c)_{32} = 0.75$$

$$(t/c)_{12}^* = (t/c)_{22}^* = (t/c)_{32}^* = 5.9\%$$

D. Aerodynamic Constraints and Penalties

1) The aerodynamic constraint is $C_M \geq C_M^*$, where C_M^* is equal to the pitching moment value of the original geometry.

2) The unconstrained pitching moment value is $C_M \geq -\infty$.

3) Based on the authors' aerodynamic experience, it is assumed that if the value of C_M corresponding to the optimal geometry is not satisfied by the aerodynamic constraint in item 1, the pseudo trim-drag penalty will be equal to 1 aerodynamic drag count per 0.01 in ΔC_M .

IV. Optimization Tools

Three different optimization tools were used to solve the drag minimization problem: SYN107, MDOPT, and OPTIMAS. Brief descriptions of these optimization methods are presented subsequently.

A. Optimization Tool SYN107

The optimization tool SYN107 employs a gradient-based search method. In the gradient calculation, a cost-effective technique is used in which the gradient is computed through the solution of an adjoint equation to the continuous Reynolds-averaged Navier–Stokes (RANS) equations, such as that developed in [13]. The design space is automatically established by treating the geometry as a free surface, with thousands of design variables linked to the discrete surface points of the computational grid. This design space is then navigated toward a local minimum by recasting the gradient in a Sobolev space. This significantly reduces the number of design cycles required to reach convergence of the optimum shape. A SYN107 optimization costs about one order of magnitude more than an objective function evaluation.

The essential idea may be summarized as follows. For flow about an arbitrary body, the aerodynamic properties that define the cost

function I are functions of flowfield variables w and the physical shape of the body, which may be represented by the function F . Then

$$I = I(w, F)$$

and a change in F results in a change of the cost function:

$$\delta I = \frac{\partial I^T}{\partial w} \delta w + \frac{\partial I^T}{\partial F} \delta F$$

Using a technique drawn from control theory, the governing equations of the flowfield are introduced as a constraint in such a way that the final expression for the gradient does not require reevaluation of the flowfield. To achieve this, δw must be eliminated from the preceding equation. Suppose that the governing equation R , which expresses the dependence of w and F within the flowfield domain D , can be written as

$$R(w, F) = 0 \quad (4)$$

Then δw is determined from the equation

$$\delta R = \frac{\partial R}{\partial w} \delta w + \frac{\partial R}{\partial F} \delta F = 0$$

Next, introducing a Lagrange multiplier Ψ with some rearrangement and choosing Ψ to satisfy the adjoint equation

$$\left[\frac{\partial R}{\partial w} \right]^T = \frac{\partial I}{\partial w} \quad (5)$$

the term multiplying δw can be eliminated in the variation of the cost function, and we find that

$$\delta I = G \delta F \quad (6)$$

where

$$G = \frac{\partial I^T}{\partial F} - \Psi^T \left[\frac{\partial R}{\partial F} \right]$$

The advantage is that the variation in cost function is independent of δw , with the result that the gradient of I with respect to any number of design variables can be determined without the need for additional flowfield evaluation.

The cost of solving the adjoint equation is comparable with that of solving the flow equation. Hence, the cost of obtaining the gradient is comparable with the cost of two function evaluations, regardless of the dimension of the design space.

Based on this property of the search method, the optimization tool SYN107 automatically sets up the design space by allowing every grid point on the surface to float normal to the surface. More details concerning the tool SYN107 may be found in [14–21].

B. Optimization Tool MDOPT

MDOPT is a multidisciplinary design optimization tool developed at The Boeing Company for air vehicle design and analysis [22]. The MDOPT system contains a collection of technology modules for performing optimization studies by means of a graphical user interface (GUI) and combining a set of in-house robust numerical optimization schemes (Design Explorer [23]) with higher-order computational analysis. Global or local direct-driven design optimizations may be completed using a variety of multidisciplinary objective and constraint functions including aerodynamics, weight, mission performance, and stability and control characteristics.

The MDOPT system is characterized by its scalability (which enables the user to frame its application to fit available schedule requirements and computing resources), its flexibility (which enables the user to choose from a variety of solvers and other computer-aided engineering tools), and its extensibility (which enables the system to grow through refinement of existing capabilities and the incorporation of new ones: for example, the

incremental incorporation of additional analysis disciplines or capabilities to address increased geometric complexity).

A general outline of the steps required in performing an optimization with MDOPT is the following. First, the geometry is input into the system and surface grids, or lofts, are created for the input geometry. Next, the user defines the design variables and selects a design of experiments. For each design point in the experiment, geometry perturbations are created and run through each of the discipline analysis codes. Geometric constraint checks are performed, and interpolated response surfaces (IRS) are created for the constraints and objective functions. Optimization and IRS model refinement are then performed on these IRS models, and the final optimum geometry and design vector are output. As an alternate to IRS model optimization and refinement, a direct-driven (DD) approach is also provided, wherein design-variable sensitivities are directly approximated using the finite difference method, from calls to the flow solver, rather than to an IRS model. DD can be used to locate a local optimum once IRS model identifies the neighborhood of the global optimum.

Once initial user inputs have been completed, the system can proceed in an automated fashion. Parallelization of the optimization process was implemented within most domains, providing a capability to use large-scale multiple-CPU computing platforms in a computationally efficient manner. The Interdomain Communication Facility (ICF) maintains the underlying process control [24]. It is constructed using TCL1 scripts, the MICO2 CORBA Orb, and the Combat3 TCL to CORBA4 Bridge. Transfer of user input information is achieved through a master name-list file and parser utilities that extract or modify name-list parameter definitions as needed throughout the process. This name-list file also acts as the conduit between the GUI, the ICF, the Database Management Facility (DMF), and the discipline domain control scripts. All persistent user data (i.e., data created by the system) are stored into a MDOPT database via DMF utilities and MySQL5, with the exception of large binary computational model files (e.g., flow solver restart files), which are maintained separately within the system directory structure.

Design variables were chosen for this study to give as much flexibility to the solution as possible and to ease the resolution of geometric constraints. In total, 35 design variables were maintained throughout the study, for consistency. Each design variable was constrained by its minimum and maximum values; however, never in any of the optimizations did an optimum result with any of the design variables at their extremes. The minimum and maximum values were chosen, for the most part, as $\pm 20\%$ of the baseline value for each design variable to assure some degree of reasonableness in the resulting geometries. These values are perturbations added to the baseline geometry and, as such, the baseline design vector consists of 35 zeros.

There are 4 design stations: nominally, the root, the tip, and the 40 and 75% spans. Twist is varied independently at each of the three most outboard design stations. Camber- and thickness-perturbation classical splines are specified at each of the design stations and are given as a fraction of the chord. Each spline is defined by three knots located at 25, 47.5, and 75% chord. There are also two implied knots at 0 and 100% chord, where the perturbation is zero. The minimum value of the thickness spline at 25 and 75% chord is set to zero to satisfy the spar thickness constraint. Thus, the thickness at these two chord locations can never be less than the baseline.

To give the designer more control over leading- and trailing-edge camber, a leading-edge- and trailing-edge-deflection design variable is given at each design station in degrees. The leading-edge hinge line is at 10% chord and the trailing-edge hinge line is at 85% chord.

C. Optimization Tool OPTIMAS

The optimization tool OPTIMAS uses a genetic algorithm as its search engine. Genetic algorithms (GAs) became highly popular as optimization methods in the last two decades. The basic idea behind genetic algorithms is to mathematically imitate the evolution process of nature. They are semistochastic optimization methods that are

conveniently presented using the metaphor of natural evolution. As a basic algorithm, a variant of the floating-point GA is employed [25]. We used the tournament selection, which enables us to increase the diversity of the parents. Three types of crossover operator were employed: single-point, uniform, and arithmetical crossover. We applied the nonuniform mutation as the mutation operator.

To improve the computational efficiency of the GA search algorithm, we use a reduced-order-model approach in the form of a local approximation method in which the solution functionals are approximated by a local database. The database is obtained by solving the full Navier–Stokes equations in a discrete neighborhood of a basic point (basic geometry) positioned in the search space. Additionally, to ensure the global character of the search, we perform iterations in such a way that in each iteration, the result of optimization serves as the initial point for the next iteration step (further referred to as optimization step).

In the present work, the shape of the wing is generated by a linear spanwise interpolation between 2-D sectional cuts. For approximation of the upper and lower cut surfaces, Bézier-spline representations are used. Summing up, the set of design parameters consists of Bézier-spline coefficients, twist angle, and dihedral value for all design sections. In total, 55 design variables were used in the present test case.

More details concerning the tool OPTIMAS may be found in [7,26], in which the aerodynamic designs of 3-D isolated transport-type wings were presented.

V. CFD Drivers

All of the preceding described optimization tools used the numerical solution of Reynolds-averaged Navier–Stokes equations as a CFD driver of the optimization stream. The mesh sizes in the fine level (used in the analysis runs) were chosen based on the results of grid convergence studies for the corresponding RANS solvers (see [27–29]); these data are presented in Table 1.

The corresponding RANS solver for design tool SYN107 was a multigrid/multiblock structured code FLO107. This code uses a cell-centered finite volume numerical scheme with the H-CUSP scheme for convective fluxes and central discretization for viscous fluxes, Runge–Kutta local time-stepping, and implicit residual smoothing. The computational grids contained 4 multigrid levels. Each level included either 8 or 12 blocks, depending on the computer. Based on a grid convergence study, the total number of grid points in the fine-level mesh was 818,545. More details concerning the code FLO107 may be found in [20,21].

The CFD driver for MDOPT was the NASA Langley Research Center solver TLNS3-D ([27]). Thin-layer Reynolds-averaged Navier–Stokes equations are solved using a five stage Runge–Kutta time-integration scheme. A finite volume scheme based on Jameson’s [30] approach is employed to construct both viscous and inviscid fluxes. Matrix dissipation is added to enhance numerical stability, and a multigrid scheme is used to accelerate convergence rate. Although several turbulence models are available in the code, the Spalart–Allmaras model was used throughout this analysis [31]. The entire flowfield is treated as fully turbulent. A robust, reliable, accurate, and fast method is desirable for optimization calculations and TLNS3-D seems to fit the bill, especially for geometries that can be gridded with a simple single-block grid.

Lift, drag, and pitching moment convergence for the baseline solution with TLNS3-D run in lift-matching mode was obtained in 300 iterations, or approximately 3 h running on a single 2.6 GHz Opteron processor. Converged solutions on the perturbed geometries, also in lift-matching mode, were obtained from restarting the baseline solution in 200 iterations, or 2 h. The

optimizations were run on an in-house cluster of dual-node Opteron processors with 4 GB RAM each and with as many as 48 solutions running in parallel during times of low cluster usage.

The baseline-wing surface grid was taken from the OVERFLOW analysis (described subsequently in this section) up to the reference wing tip. The tip was closed by an in-house method that generates a rounded closed tip with a maximum radius equal to half the wing-tip thickness and adds 5 spanwise grid planes. Surface perturbations for each design point are calculated by routines within MDOPT. A single-block C-H volume-grid topology is used with 41 axial points in the wing trailing wake and 41 spanwise points from the wing tip to the far field. The wing wake is closed at the first point off the wing surface and no grid points are located along the blunt trailing edge. It was shown that this handling of the wake grid in a single-block grid gives the most similar solution to a full multiblock OVERFLOW solution with a grid on the blunt trailing edge. The downstream far field is located at about 12.5 reference chord lengths aft of the wing trailing edge, and the spanwise far field is at approximately 3.3 reference span lengths outboard of the wing tip. The baseline volume grid is generated by LEGRID (a variant of HYPGEN [32]) and the perturbed-geometry volume grids are generated by CSCMDO [33]; both are within the MDOPT framework. There are 81 points normal to the surface clustered for a boundary layer at the design Reynolds number with the far field at approximately 12.5 reference chord lengths from the surface. There are 225 points around the wing airfoil surface, and the wing tip is at the 105th spanwise plane. The full volume grid consists of 3,582,225 points, with dimensions of $305 \times 145 \times 81$.

Numerical solutions of RANS equations in the framework of the optimization tool OPTIMAS were based on the structured multiblock/multiface code NES [28,34], which employs the essentially nonoscillatory (ENO) concept with a flux interpolation technique that allows accurate estimation of sensitive aerodynamic characteristic such as lift, pressure drag, friction drag, and pitching moment. The effects of turbulence are modeled through an eddy-viscosity hypothesis with the Baldwin–Lomax turbulence model [35].

To accelerate the convergence to the steady state, a defect-correction multigrid approach is used that employs a first-order-accurate driver and a high-order ENO defect correction. Nonlinear stability is maintained via approximation of inviscid fluxes on a variable template according to local characteristics and smoothness of the fluxes; viscous fluxes are approximated in a straightforward way. The resulting multigrid method retained the high accuracy of the ENO approach with a comparatively small number of multigrid cycles needed to reduce the error below the level of truncation errors. Additionally, to improve the computational efficiency of the algorithm, the multilevel parallelization strategy was employed [36,37]. The computational grids contained three multigrid levels; each level included 4 blocks. The total number of points in the fine level was about 250,000.

CFD solutions using the NASA code OVERFLOW were used to provide an unbiased comparative analysis (relative to the optimizers’ own solutions) of the optimized geometries. OVERFLOW [38] is a node-based Reynolds-averaged Navier–Stokes flow solver that can calculate solutions of complex geometries by using multiple-structured overset-grid topologies. The Boeing solutions were generated using the message-passing interface OVERFLOW (version 2.0z, with 64-bit precision) and using grid sequencing for accelerated convergence. The one-equation Spalart–Allmaras [31] turbulence model was used, and the solutions did not incorporate the thin-layer approximations. A second-order Roe upwind numerical differencing scheme was used.

Solutions for the DPW-W1 [39] and optimized geometry solutions used a three-block grid topology composed of a wing grid, trailing-edge cap grid, and wing-tip cap grid. The total grid-point count for the computational domain was approximately 4 million nodes. All surface- and volume-grid construction practices were in accordance with the methods outlined by Vassberg et al. [29]. Near-wall y^+ spacing of 1 was maintained for all viscous wall grids. Wing surface-grid chordwise spacing was clustered to a length of 0.1% local chord

Table 1 Grid sizes in the fine level for the different RANS solvers

RANS solver	FLO107	TLNS3-D	NES	OVERFLOW
Grid size	818,545	3,582,225	250,000	4,000,000

at both the leading and trailing edges. The wing grid was coupled with a wake that extended downstream a distance equal to the wing reference chord. The total wing/wake surface grid was composed of 289 points in the streamwise direction, and the spanwise spacing had 101 total points. The wing trailing-edge base was modified with an overset grid to incorporate a total of 13 chordwise cells and maintained the same spanwise spacing as the wing grid. The wing-tip cap overset grid maintained the wing grid streamwise point spacing and closed out the tip by rounding the wing surface over. The outer computational boundaries were placed away from the wing grid at a distance equal to 35 times the reference chord length.

VI. Analysis of Results

A. SYN107 Results

A total of 3 optimizations were performed. The design conditions and constraints are summarized in Table 2. The corresponding optimal shapes are designated as case S4 to case S6. The thicknesses of the optimal wings were greater than or equal to the original wing's thickness. The results of flow analysis in terms of the absolute values of C_D and C_M at $C_L = 0.5$ for $M = 0.76$ and 0.78 are presented in Table 3.

Results of the optimizations that were penalized with respect to C_M were as follows. The one-point optimization case S4 (design Mach $M = 0.76$) yielded drag reduction of 12.9 aerodynamic counts, whereas at an offdesign Mach $M = 0.78$, the drag reduction was equal to 3.0 counts. In turn, the one-point optimization at the design Mach $M = 0.78$ (case S5) reduced the original drag value by 29.8 counts, whereas at an offdesign $M = 0.76$, the corresponding drag reduction was equal to 3.7 counts. The three-point optimization case S6 reduced the total drag by 10.5 counts at $M = 0.76$ and by 26.3 counts at $M = 0.78$. Interestingly, if one adds the 12.9 count

improvement of case S4 with the 29.8 count benefit of case S5, a threshold level of 42.7 counts is established. This level represents an upper bound to the aggregate improvement that can be achieved by a multipoint design at these two flow conditions. The aggregate improvement from case S6 is 36.8 counts. Hence, this multipoint optimization recovered over 86% of its maximum potential improvement.

B. MDOPT Results

A total of 5 optimizations were performed. The design conditions and constraints are summarized in Table 4. The corresponding optimal shapes are designated by case M1, case M5, case M7, case M8A, and case M9. The first two cases deal with one-point optimization at the design Mach $M = 0.76$, and the last three cases perform dual-point optimization. All cases include the spar thickness constraints at $x/c = 0.2$ and 0.75 , as described in the preceding design-variable section, and all constrain the maximum airfoil thickness to be no less than the DPW-W1 wing. Some cases were run with sequential response-surface model optimization and refinement, SEQOPT, whereas others were run with a DD optimization scheme. The results of flow analyses (TLNS3-D) in terms of the absolute values of C_D and C_M at $C_L = 0.5$ for $M = 0.76$ and $M = 0.78$ are presented in Table 5.

Case M1 was basically a shakeout run to get the MDOPT system working efficiently on our computer cluster and to determine the best settings for various parameters that control the optimization and model refinements. The first case therefore took an inordinate amount of time to complete. It achieved an 11.8 count improvement over the baseline, but with a significant increase in nose-down pitching moment. When the nose-down pitching moment penalty was included in the cost function, case M5 was able to achieve the same amount of drag reduction as case M1 did; however, it did so with less nose-down pitching moment.

Note that these two cases only differ with respect to the optimization method. Generally, it takes twice as many flow code evaluations for the SEQOPT cases as with the direct-driven cases to reach an optimum; however, the time to get a final solution is comparable because more of the flow code evaluations in SEQOPT can be run in parallel.

Figures 1 and 2 show a comparison of the resulting pressure distributions and span loads for case M1 and case M5 compared with the baseline. MDOPT was successful in significantly reducing the

Table 2 Optimization conditions and constraints for the DPW-W1 wing alone with SYN107

Case no.	C_L^*	M	Beam	C_M^*
Case S4	0.50	0.76	Yes	C_M^{orig}
Case S5	0.50	0.78	Yes	C_M^{orig}
Case S6	0.50	0.76	Yes	C_M^{orig}
	0.50	0.77	Yes	C_M^{orig}
	0.50	0.78	Yes	C_M^{orig}

Table 3 Estimation of C_D and C_M by the code FLO107 for the original DPW-W1 wing vs optimal geometries achieved by the optimization tool SYN107

Case no.	$M = 0.76$		$M = 0.78$	
	C_D	C_D	C_M	C_M
DPW-W1	222.3c	244.9c	-0.0734	-0.0834
Case S4	209.4c	241.9c	-0.0669	-0.0764
Case S5	218.6c	215.1c	-0.0771	-0.0842
Case S6	211.8c	218.6c	-0.0750	-0.0834

Table 5 Estimation of C_D and C_M by the code TLNS3-D for the original DPW-W1 wing vs optimal geometries achieved by the optimization tool MDOPT

Case No.	$M = 0.76$		$M = 0.78$	
	C_D	C_D	C_M	C_M
DPW-W1	223.1c	247.6c	-0.0714	-0.0812
Case M1	211.3c	—	-0.0889	—
Case M5	211.4c	241.5c	-0.0784	-0.0867
Case M7	216.0c	219.6c	-0.1000	-0.1071
Case M8A	214.1c	217.1c	-0.1067	-0.1142
Case M9	214.3c	218.7c	-0.0860	-0.0935

Table 4 Optimization conditions and constraints for the DPW-W1 wing alone with MDOPT

Case no.	C_L^*	M	Beam	C_M^*	Opt. type	No. runs	CPU days
Case M1	0.50	0.76	Yes	$-\infty$	Seq	1404	26
Case M5	0.50	0.76	Yes	C_M^{orig}	DD	412	6
Case M7	0.50	0.76	Yes	C_M^{orig}	DD	1030	18
	0.50	0.78	Yes	C_M^{orig}	—	—	—
Case M8A	0.50	0.76	Yes	$-\infty$	Seq	1214	4
	0.50	0.78	Yes	$-\infty$	—	—	—
Case M9	0.50	0.76	Yes	C_M^{orig}	Seq	2676	14
	0.50	0.78	Yes	C_M^{orig}	—	—	—

DPW-W1 MDOPT/TLNS

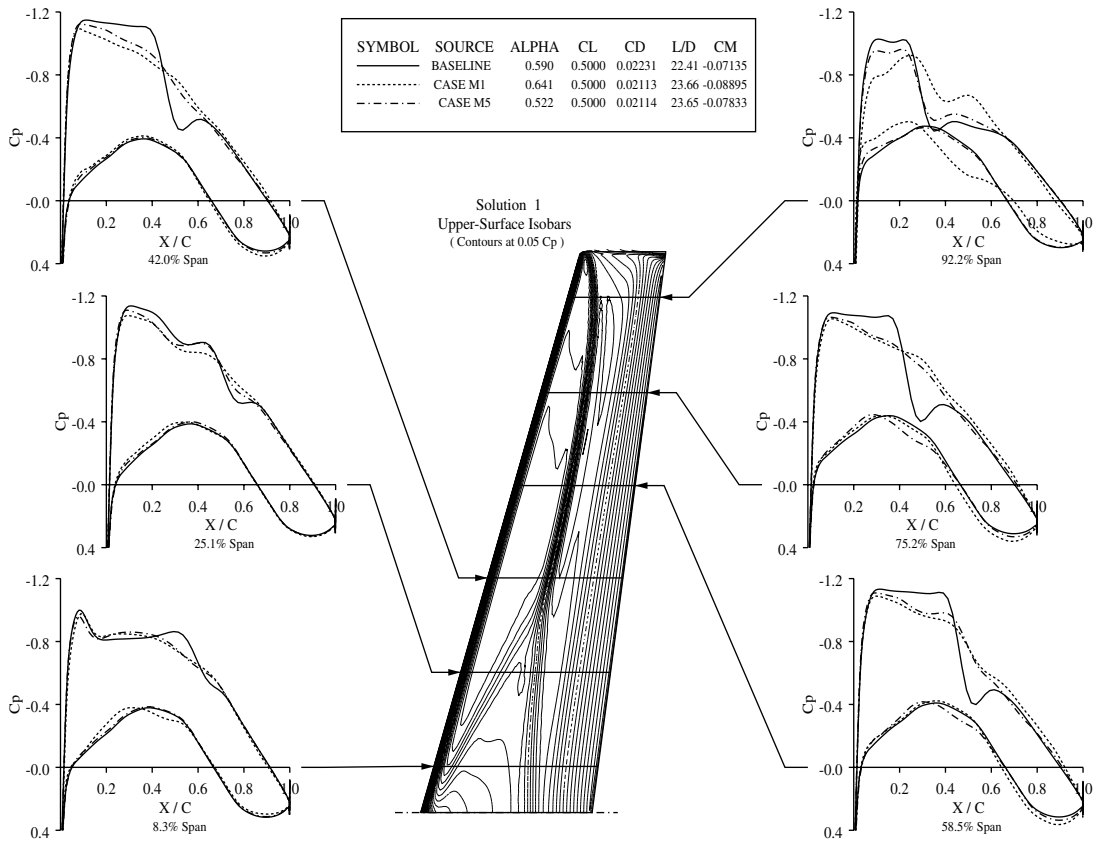


Fig. 1 Comparison of chordwise pressure distributions for case M1 and case M5 at $M = 0.76$ and $Re = 5.0 \times 10^6$.

DPW-W1 MDOPT/TLNS

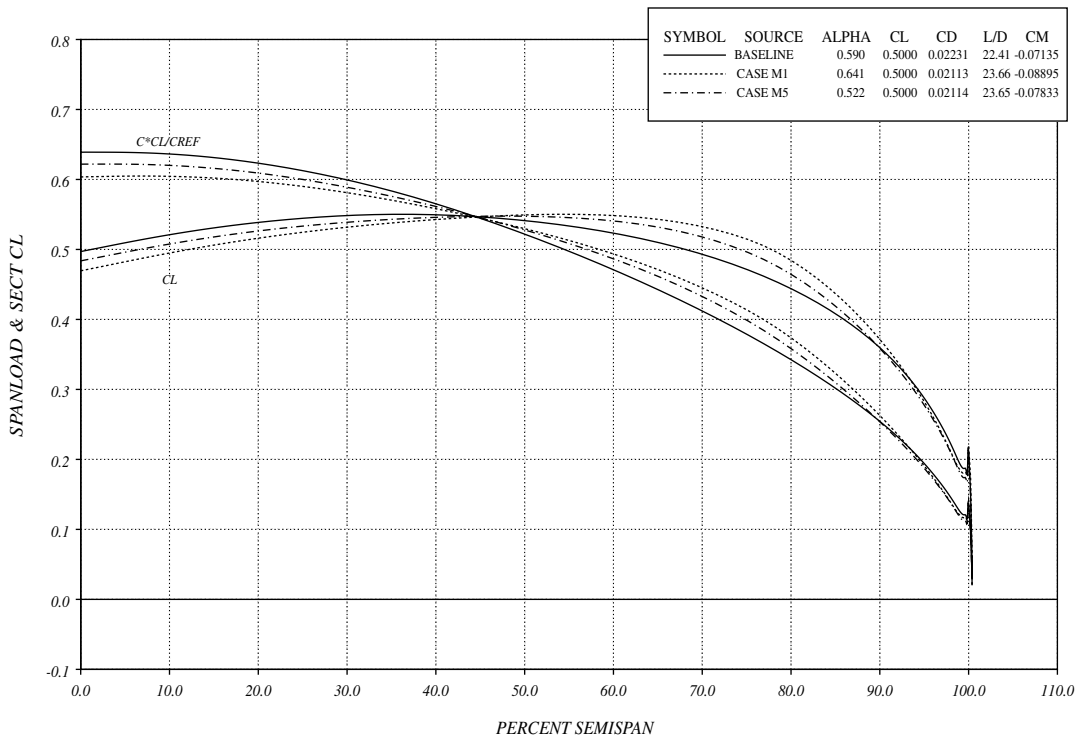


Fig. 2 Comparison of span-load distributions for case M1 and case M5 at $M = 0.76$ and $Re = 5.0 \times 10^6$.

shock strength as well as moving the span load outward for a wave and induced-drag benefit. The effect of the pitching moment penalty did not allow the span load to move outboard as much as for case M1, and each sectional pressure distribution showed a tendency toward less nose-down moment.

The results of optimization stress the importance of achieving a well-converged solution. With the SEQOPT method in particular, which tends to find improvements in a stepwise manner, it is particularly prudent to let it run for a significant number of cycles past what one might think is a converged solution. It is possible for it to find a better local minimum and step to it as the response-surface model is refined.

The multipoint design cases with pitching moment penalty used in the cost function, case M7 and case M9, differ by the starting geometry. Case M7 starts from the baseline, whereas case M9 starts from the resulting geometry of case M5 to determine if it is possible to reach the single-point optimum at the lower Mach number. The corresponding comparisons of the resulting pressure distributions and span loads for two-point optimizations are given in Figs. 3–6.

At both Mach numbers, the decrease in drag and drag corrected for pitching moment are better than or equal to the cases with no pitching moment penalty. It is also noted that the single-point optimum at the lower Mach number is not achieved. The pressure distributions show that for both cases, the shock strength at the lower Mach number was not as successfully reduced as in the single-point optimization; however, significant improvement is seen at the higher Mach. At the higher Mach, MDOPT seems to have traded a strong shock at the wing tip with two weaker shocks.

This double-shock behavior is intuitively undesirable and may leave room for additional improvement. MDOPT may have been limited in this sense by the choice of design variables that may have constricted the changes desired near the tip. Both cases show an outboard shifting of the span load at both Mach numbers as in the

single-point optimization cases, indicative of an induced-drag benefit.

C. OPTIMAS Results

We next present applications of the tool OPTIMAS to the solution of the preceding specified test cases. A total of 3 optimizations were performed. The design conditions and constraints are summarized in Table 6. The corresponding optimal shapes are designated as case O3 to case O5. The average number of optimization steps needed to reach convergence was equal to 8. On the computer cluster with 108 processors, it took about 16 wall-clock hours. The results of flow analysis in terms of the absolute values of C_D and C_M at $C_L = 0.5$ for $M = 0.76$ and 0.78 are presented in Table 7.

Before analyzing the results of the optimizations, let us consider the systematic comparison between NES data and OVERFLOW data for the same geometries at the main design point $M = 0.76$ and $C_L = 0.5$. The corresponding comparison is given in Table 8 for the values of viscous drag C_D^{visc} , pressure drag C_D^{pres} , and total drag C_D computed by the code NES and the code OVERFLOW. It may be concluded that the two codes yield very similar drag results in terms of both viscous and pressure drag for a wide range of tested geometries. Specifically, on average, the difference between C_D values by these two codes is about 1 count.

At the main design point, the drag of the original wing is 217.8 aerodynamic counts. In case O3, the optimization yielded 200.7 drag counts ($C_M = -0.129$); in case O4, the total drag was equal to 204.3 counts, whereas the pitching moment was kept to the original level ($C_M = -0.071$). A detailed analysis of the results allows us to conclude that both of the optimized wings feature shockless behavior. Note that the corresponding drag values are very close to the theoretical minimum ($C_{D_0} + C_D^{induced}$, where C_{D_0} is equal to the minimum drag value of the initial wing).

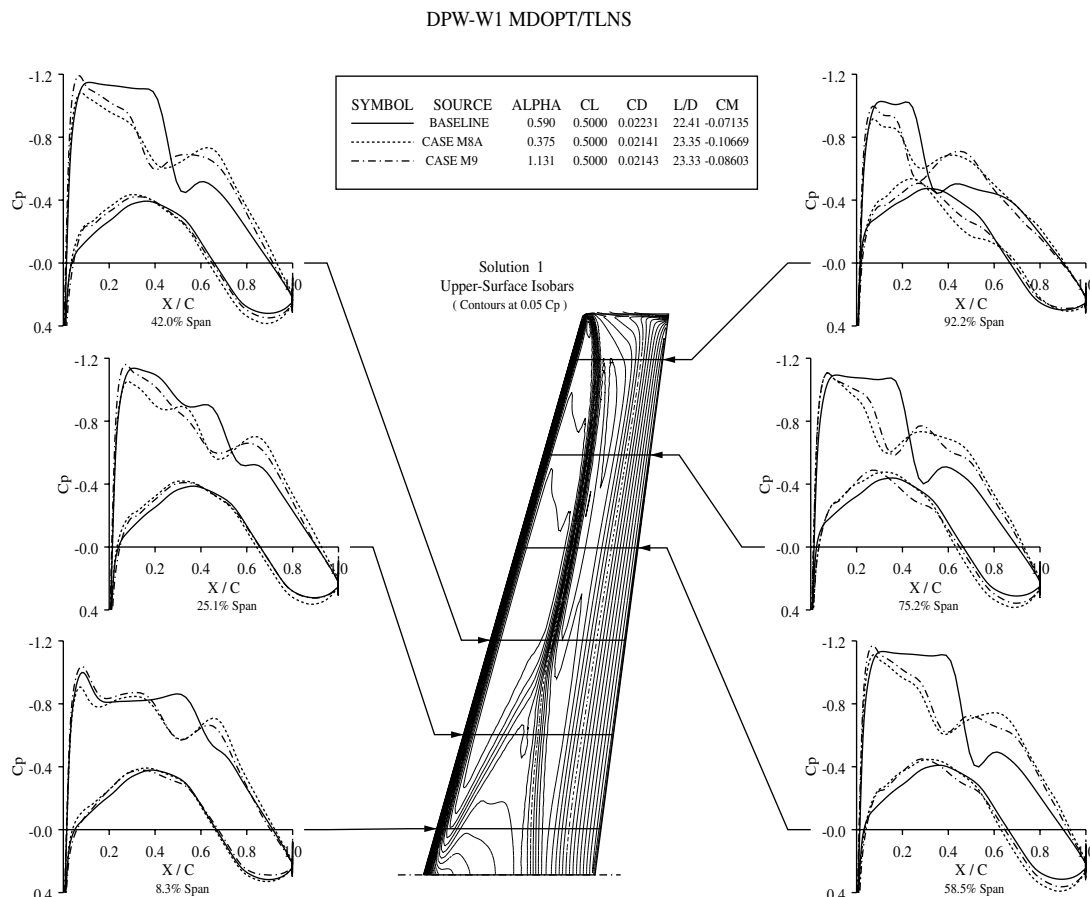


Fig. 3 Comparison of chordwise pressure distributions for the dual-point optimization cases at $M = 0.76$ and $Re = 5.0 \times 10^6$.

DPW-W1 MDOPT/TLNS

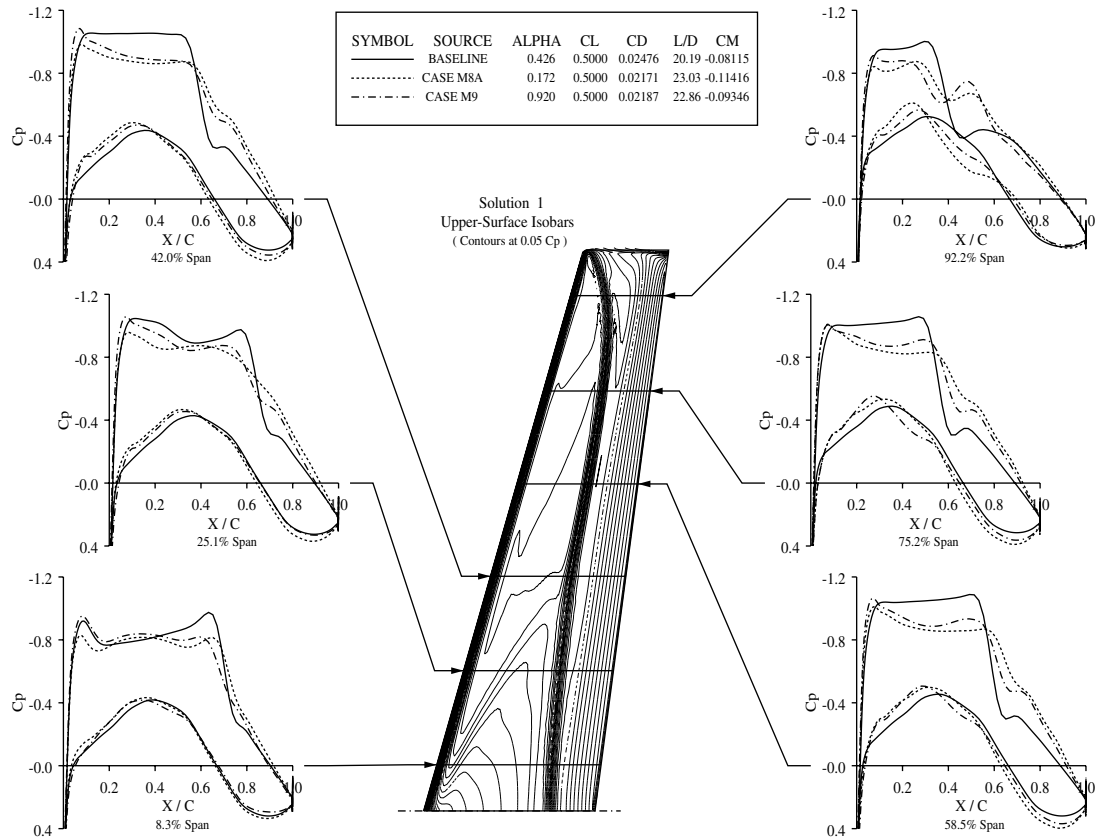


Fig. 4 Comparison of chordwise pressure distributions for the dual-point optimization cases at $M = 0.78$ and $Re = 5.0 \times 10^6$.

DPW-W1 MDOPT/TLNS

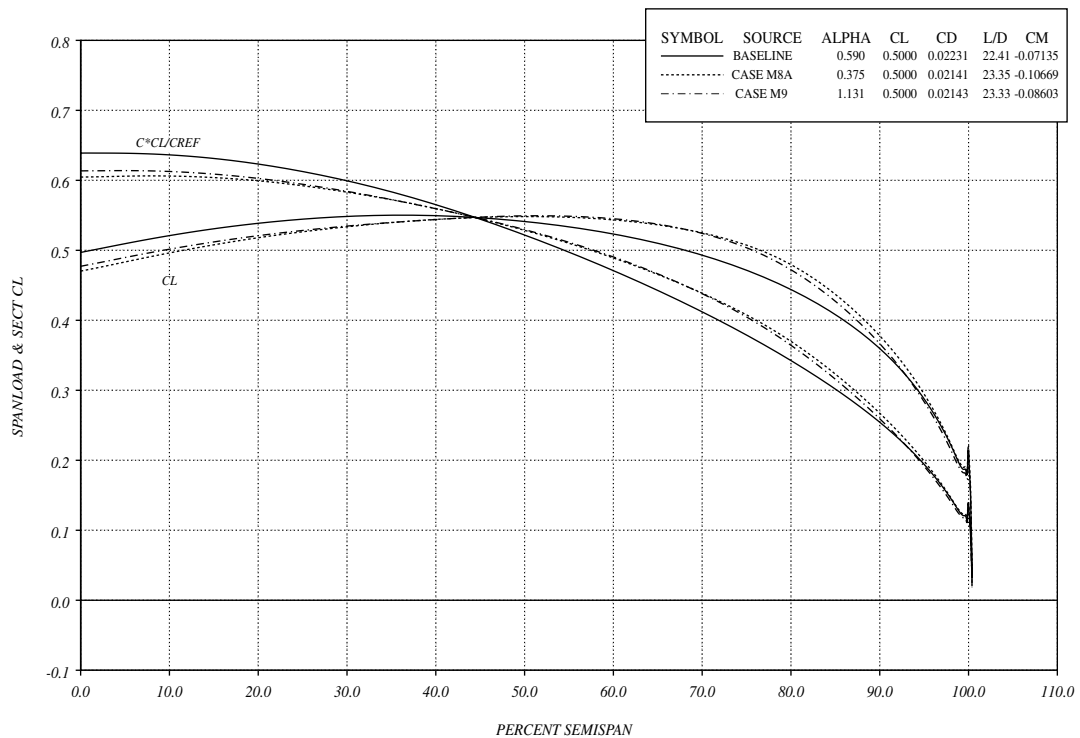


Fig. 5 Comparison of span-load distributions for the dual-point optimization cases at $M = 0.76$ and $Re = 5.0 \times 10^6$.

DPW-W1 MDOPT/TLNS

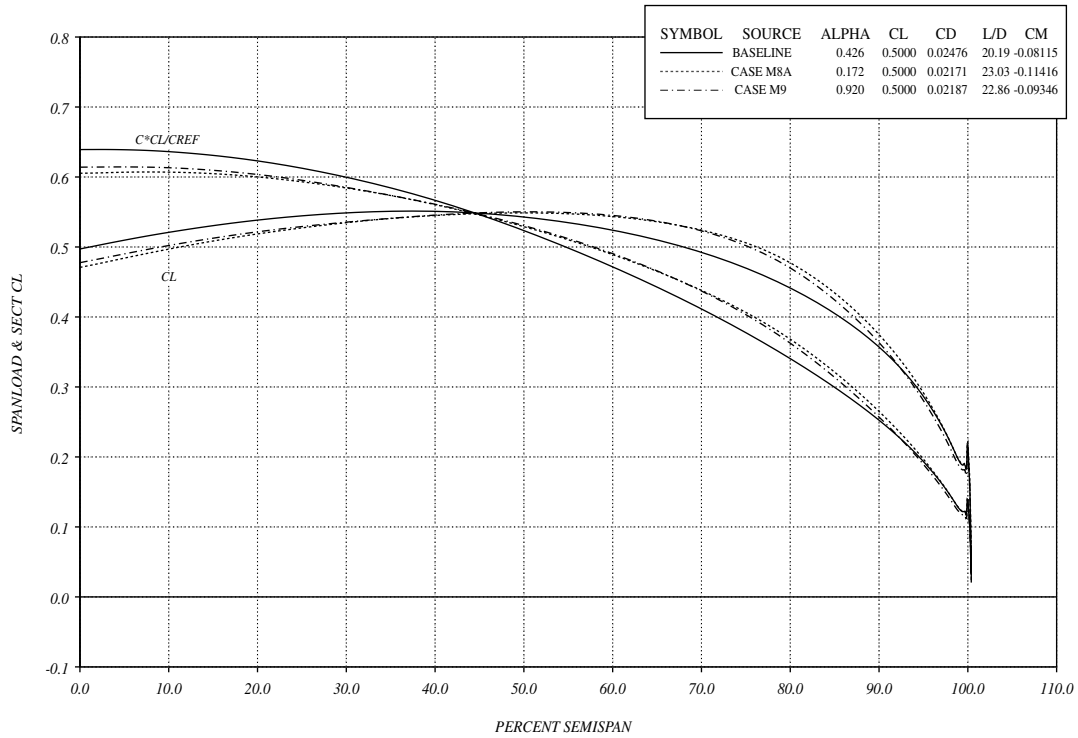


Fig. 6 Comparison of span-load distributions for the dual-point optimization cases at $M = 0.78$ and $Re = 5.0 \times 10^6$.

Table 6 Optimization conditions and constraints for the DPW-W1 wing alone with OPTIMAS

Case no.	C_L^*	M	Beam	C_M^*
Case O3	0.50	0.76	Yes	$-\infty$
Case O4	0.50	0.76	Yes	-0.071
Case O5	0.50	0.76	Yes	-0.071
	0.50	0.78	Yes	$-\infty$
	1.80	0.20	Yes	$-\infty$

Table 7 Estimation of C_D and C_M by the code NES for the original DPW-W1 wing vs optimal geometries achieved by the optimization tool OPTIMAS

Case no.	$M = 0.76$	$M = 0.78$	$M = 0.76$	$M = 0.78$
	C_D	C_D	C_M	C_M
DPW-W1	217.8c	241.3c	-0.071	-0.081
Case O3	200.7c	221.0c	-0.129	-0.139
Case O4	204.3c	226.7c	-0.071	-0.081
Case O5	203.6c	220.5c	-0.071	-0.081

Table 8 NES computations vs OVERFLOW computations for the original DPW-W1 wing and optimal geometries achieved by the optimization tool OPTIMAS with drag values at $M = 0.76$ and $C_L = 0.5$ in aerodynamic counts

Geometry	NES	NES	NES	OVERFLOW	OVERFLOW	OVERFLOW
	C_D^{visc}	C_D^{pres}	C_D	C_D^{visc}	C_D^{pres}	C_D
DPW-W1	57.3	160.5	217.8	59.3	160.0	219.3
Case O3	58.4	142.4	200.7	60.7	140.6	201.3
Case O4	58.3	145.9	204.3	60.7	143.8	204.5
Case O5	58.2	145.4	203.6	60.7	142.5	203.2

To check offdesign behavior of the optimized geometries, numerical solutions of RANS equations were performed for a wide range of freestream Mach and C_L values. The corresponding results are given in Figs. 7 and 8, in which lift/drag polars at $M = 0.76$ and Mach drag-rise curves at $C_L = 0.5$, respectively, are depicted. It can be concluded that the optimization tool allowed good design and offdesign performance with the required incorporation of beam constraints in both cases.

It is seen that the optimized wings possess significantly lower drag values, not only pointwise, but also for all $C_L > 0.2$. The optimization also improved the M_{DD} behavior of the wings and shifted the divergence to a higher Mach number.

Finally, we present the results of a three-point optimization case O5. The weighting coefficients for this case were 0.75, 0.23, and 0.02 for the corresponding design Mach values. Note that in this test case, the requirement of a sufficiently high C_L^{max} was translated into the requirement of a low drag at the conditions close to the maximum lift of the initial DPW-W1 wing. At the main design point ($M = 0.76$ and $C_L = 0.50$), the total drag of the optimized wing for case O5 was equal to 203.6 counts, whereas the pitching moment was kept to the original level. At the high Mach secondary design point ($M = 0.78$ and $C_L = 0.50$), the resulting C_D was equal to 220.5 aerodynamic counts (compared with the original 241.3 counts). At the takeoff secondary design condition, the optimization preserved the original value of C_L^{max} at $M = 0.20$.

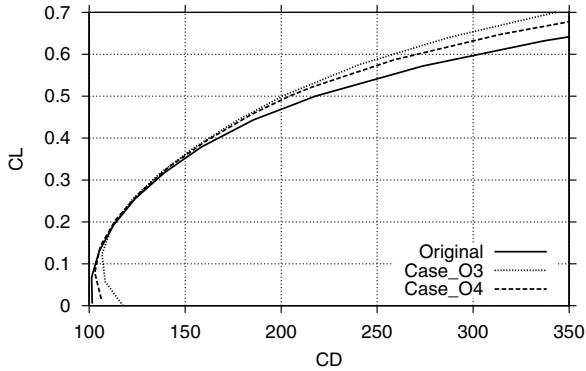


Fig. 7 Lift/drag polars at $M = 0.76$ and $Re = 5.0 \times 10^6$ for the original wing vs optimized wings.

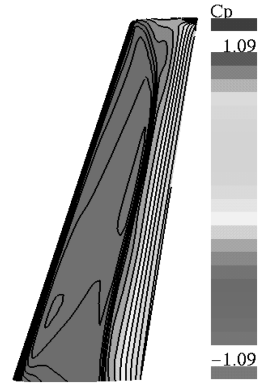


Fig. 10 Pressure distribution on the upper surface of the optimal wing for case O5 at $M = 0.78$ and $C_L = 0.50$.

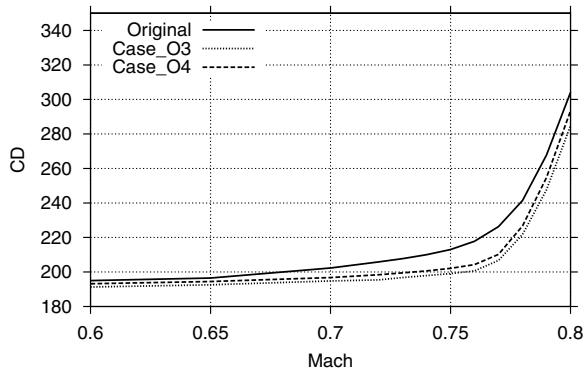


Fig. 8 Mach drag divergence at $C_L = 0.50$ for the original wing vs optimized wings.

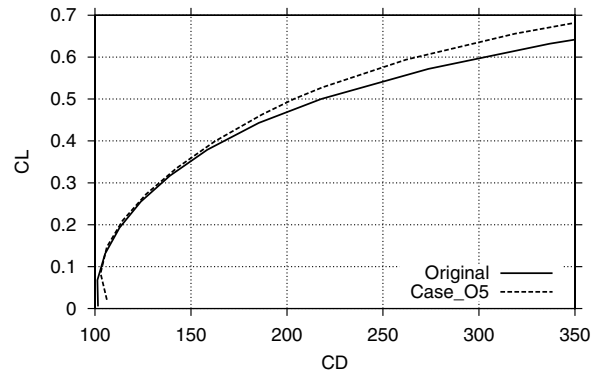


Fig. 11 Lift/drag polars at $M = 0.76$ and $Re = 5.0 \times 10^6$ for the original wing vs an optimized wing.

The pressure distribution for case O5 at $M = 0.76$ and $C_L = 0.50$ is given in Fig. 9, and the corresponding data at $M = 0.78$ and $C_L = 0.50$ for case O5 are given in Fig. 10. The data illustrating the aerodynamic performance of the optimized wing (lift/drag curves, Mach drag divergence, and C_L vs angle-of-attack curves) are shown in Figs. 11–14.

D. Cross Analysis of Optimal Wings

A systematic cross analysis was performed for the original geometry and for several optimal geometries that were generated by the optimization tools SYN107, MDOPT, and OPTIMAS. These geometries are from cases that best match the single-point and multipoint optimizations outlined in Sec. III of this paper and that were performed independently of knowledge of each of the other group’s results. In total, 4 different Navier–Stokes solvers were used in this verification study: the code TLNS3-D (the CFD driver of the

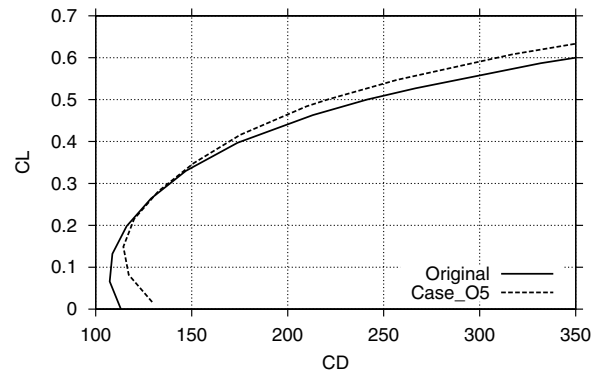


Fig. 12 Lift/drag polars at $M = 0.78$ and $Re = 5.0 \times 10^6$ for the original wing vs an optimized wing.

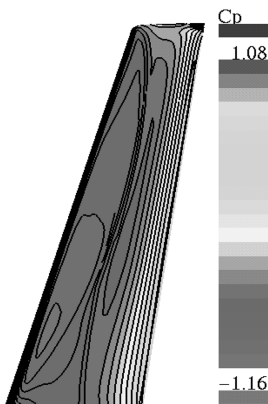


Fig. 9 Pressure distribution on the upper surface of the optimal wing for case O5 at $M = 0.76$ and $C_L = 0.50$.

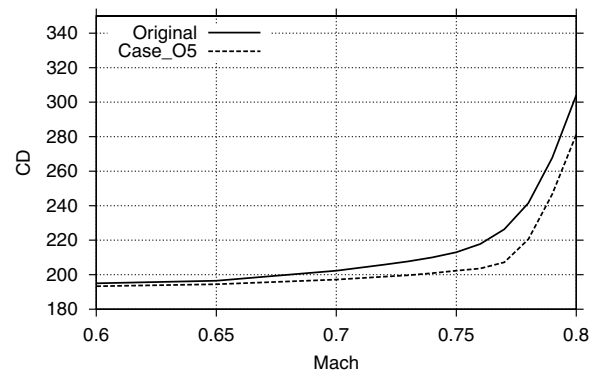


Fig. 13 Mach drag divergence at $C_L = 0.50$ for the original wing vs an optimized wing.

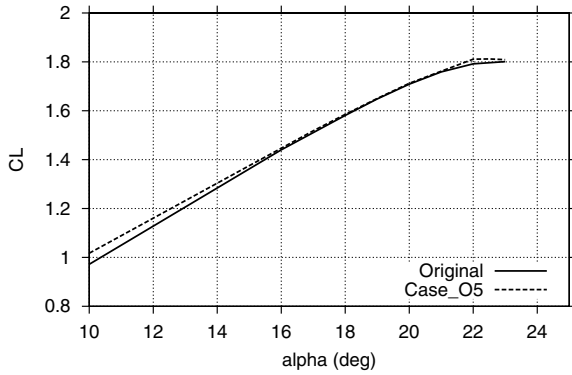


Fig. 14 C_L vs angle of attack at takeoff conditions for the original wing vs an optimized wing.

optimization tool MDOPT), the code FLO107 (SYN107), the code NES (OPTIMAS), and the code OVERFLOW.

The corresponding results are presented in Tables 9–13 and in Figs. 15–23. Table 9 contains the results of flow analysis for the original geometry (in terms of absolute values of C_D and C_M). In Tables 10–13, we find the corresponding data for the optimal geometries (in terms of drag reduction). Baseline wing-section shapes vs optimized shapes and chordwise pressure distributions (based on the OVERFLOW computations) on the optimal geometries at $M = 0.76$ and 0.78 are plotted in Figs. 15–20.

To compare the results of optimization achieved by the different optimization tools, it was agreed to correct the actual drag reduction

Table 9 Estimation of C_D and C_M by different Navier–Stokes solvers for the original-geometry DPW-W1 wing alone

Solver	$M = 0.76$		$M = 0.78$	
	C_D	C_D	C_M	C_M
FLO107	222.3c	244.9c	-0.0734	-0.0834
TLNS3D	223.1c	247.6c	-0.0714	-0.0812
NES	217.8c	241.3c	-0.0710	-0.0810
OVERFLOW	220.3c	247.0c	-0.0660	-0.0740

Table 10 Estimation of drag-reduction by the code FLO107

Case no.	$M = 0.76$		$M = 0.78$	
	ΔC_D	ΔC_D	ΔC_M	ΔC_M
Case S4	-12.9c	-3.0c	+0.0065	+0.007
Case S5	-3.7c	-29.8c	-0.0037	-0.001
Case S6	-10.5c	-26.3c	-0.002	+0.0001
Case M5	-11.0c	-6.0c	-0.0064	-0.0055
Case M7	-6.5c	-25.2c	-0.028	-0.025
Case O4	-13.9c	-15.0c	-0.009	-0.0085
Case O5	-13.8c	-20.4c	-0.011	-0.010

Table 11 Estimation of drag reduction by the code TLNS3-D

Case no.	$M = 0.76$		$M = 0.78$	
	ΔC_D	ΔC_D	ΔC_M	ΔC_M
Case S4	-13.2c	-2.8c	+0.004	+0.006
Case S5	-3.4c	-31.3c	-0.005	-0.002
Case S6	-10.4c	-27.6c	-0.004	-0.002
Case M5	-11.7c	-6.1c	-0.007	-0.006
Case M7	-7.1c	-28.0c	-0.029	-0.026
Case O4	-16.6c	-19.5c	-0.006	-0.005
Case O5	-17.4c	-25.4c	-0.008	-0.006

Table 12 Estimation of drag reduction by the code NES

Case No.	$M = 0.76$		$M = 0.78$	
	ΔC_D	ΔC_D	ΔC_M	ΔC_M
Case S4	-8.7c	-1.9c	+0.007	+0.008
Case S5	-2.7c	-22.4c	-0.0001	+0.002
Case S6	-5.7c	-19.2c	+0.001	+0.004
Case M5	-10.0c	-3.9c	-0.002	-0.002
Case M7	-8.4c	-28.7c	-0.020	-0.020
Case O4	-13.5c	-14.7c	+0.0001	-0.002
Case O5	-14.2c	-20.8c	+0.0001	-0.0001

Table 13 Estimation of drag reduction by the code OVERFLOW

Case No.	$M = 0.76$		$M = 0.78$	
	ΔC_D	ΔC_D	ΔC_M	ΔC_M
Case S4	-13.8c	-3.1c	+0.004	+0.006
Case S5	-3.8c	-31.8c	-0.003	-0.001
Case S6	-10.8c	-28.2c	-0.002	-0.001
Case M5	-14.5c	-9.0c	-0.008	-0.005
Case M7	-9.9c	-31.5c	-0.023	-0.021
Case O4	-14.8c	-16.8c	-0.003	-0.002
Case O5	-16.1c	-25.0c	-0.005	-0.003

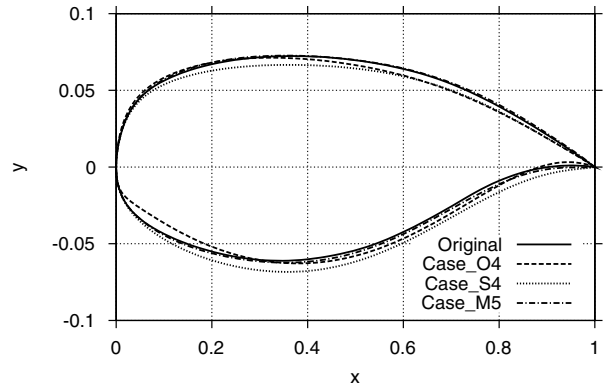


Fig. 15 DPW-W1 root shape vs optimized shapes achieved by one-point optimizations.

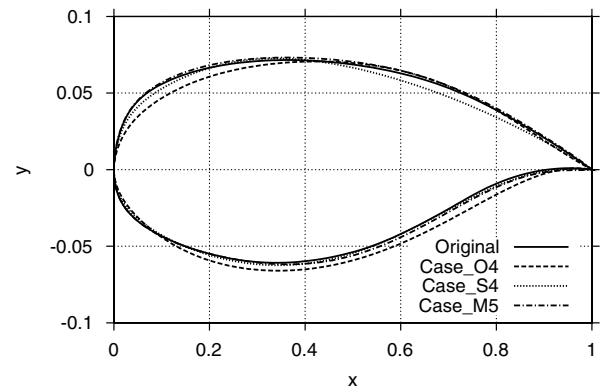


Fig. 16 DPW-W1 tip shape vs optimiz shapes achieved by one-point optimizations.

SINGLE-POINT OPTIMIZATIONS OF DPW-W1 WING

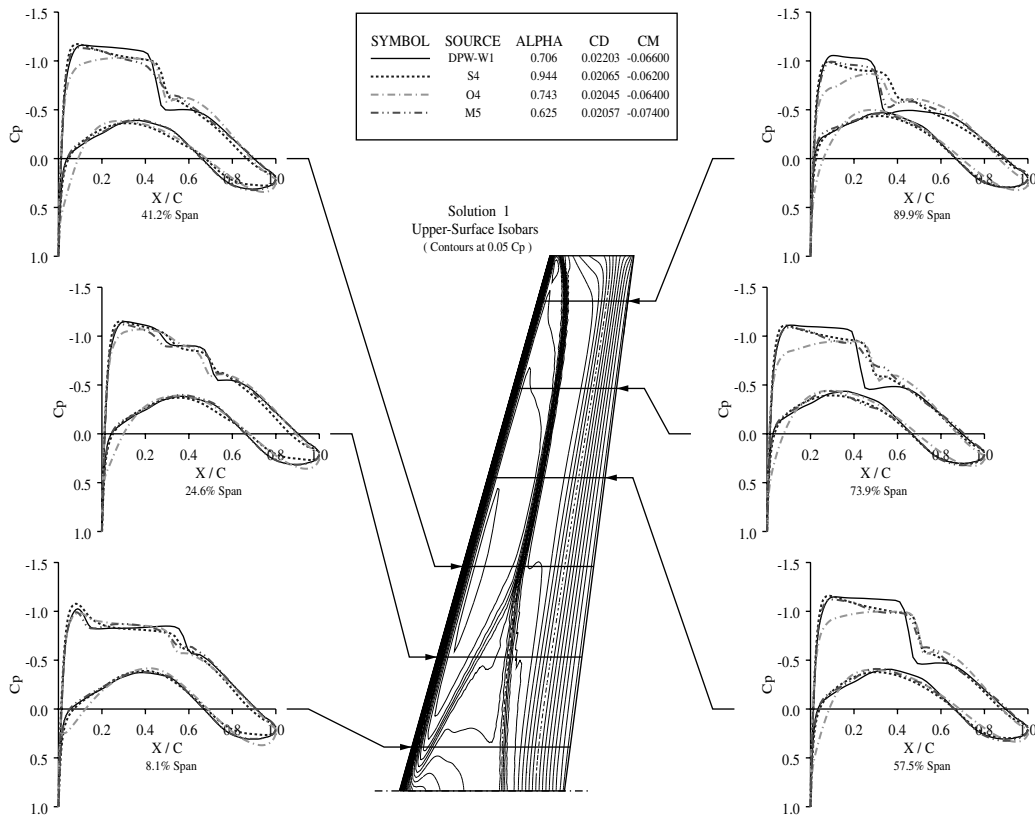


Fig. 17 Comparison of chordwise pressure distributions at $M = 0.76$, $C_L = 0.5$, and $Re = 5.0 \times 10^6$ for one-point optimization cases with OVERFLOW computations.

SINGLE-POINT OPTIMIZATIONS OF DPW-W1 WING

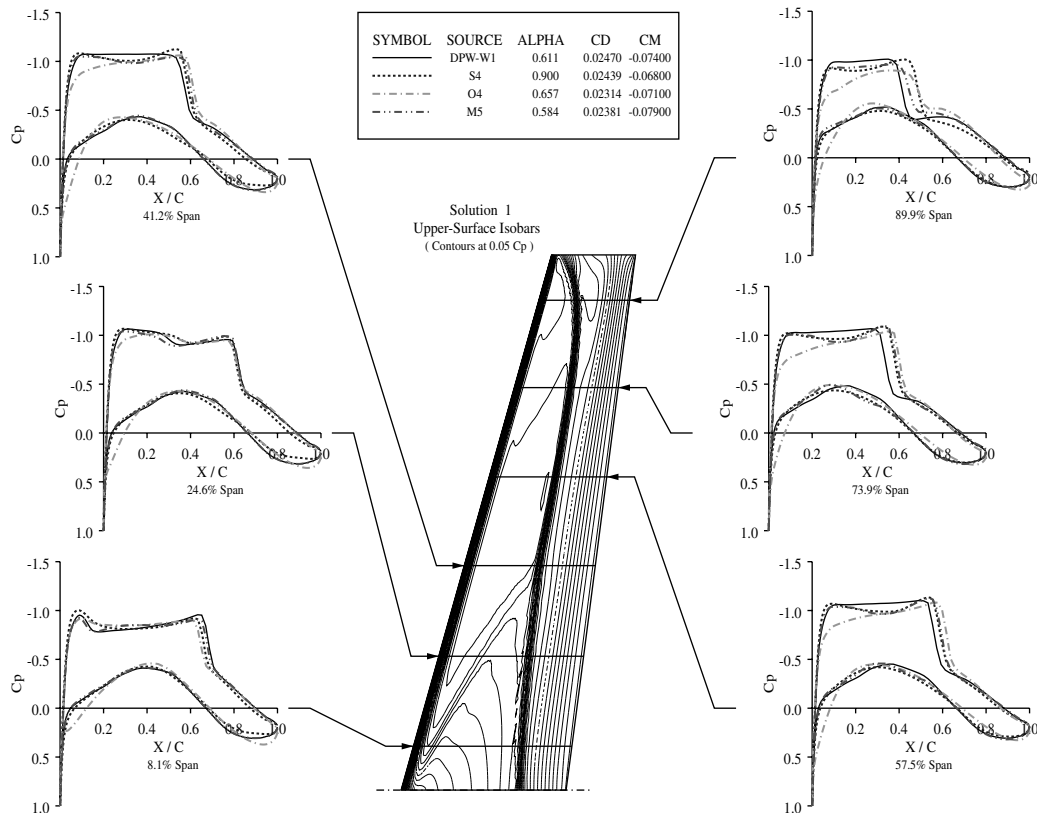


Fig. 18 Comparison of chordwise pressure distributions at $M = 0.78$, $C_L = 0.5$, and $Re = 5.0 \times 10^6$ for one-point optimization cases with OVERFLOW computations.

MULTI-POINT OPTIMIZATIONS OF DPW-W1 WING

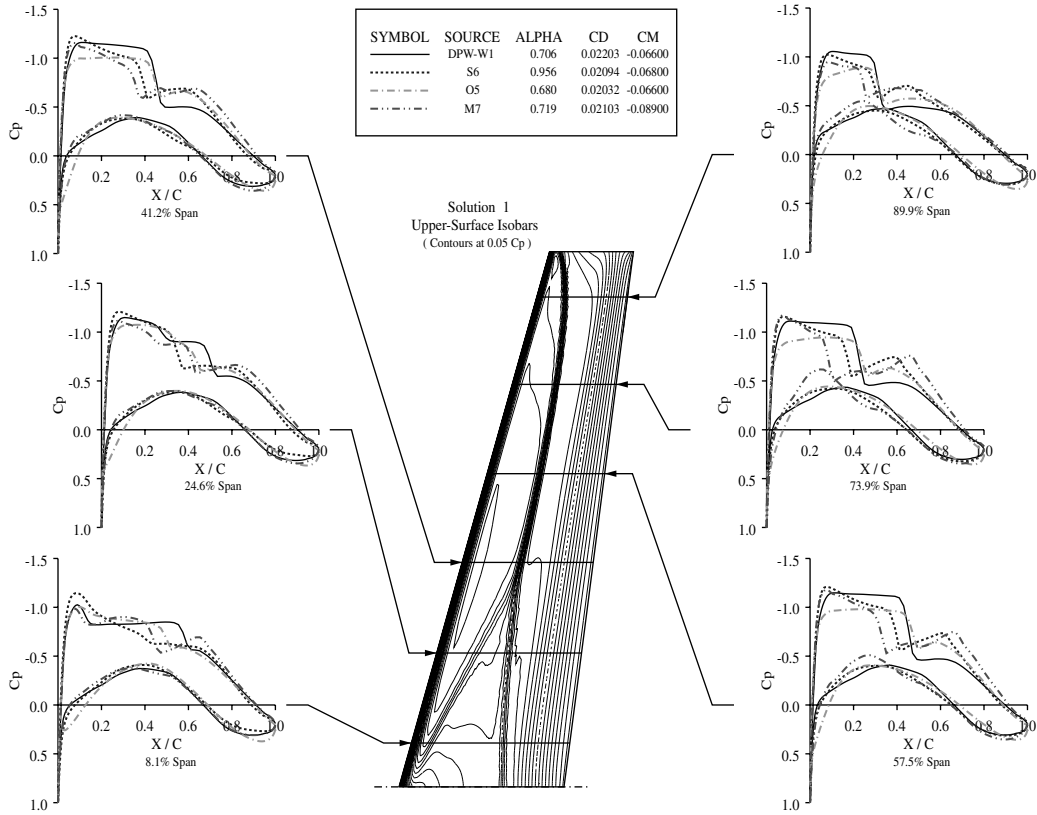


Fig. 19 Comparison of chordwise pressure distributions at $M = 0.76$, $C_L = 0.5$, and $Re = 5.0 \times 10^6$ for multipoint optimization cases with OVERFLOW computations.

MULTI-POINT OPTIMIZATIONS OF DPW-W1 WING

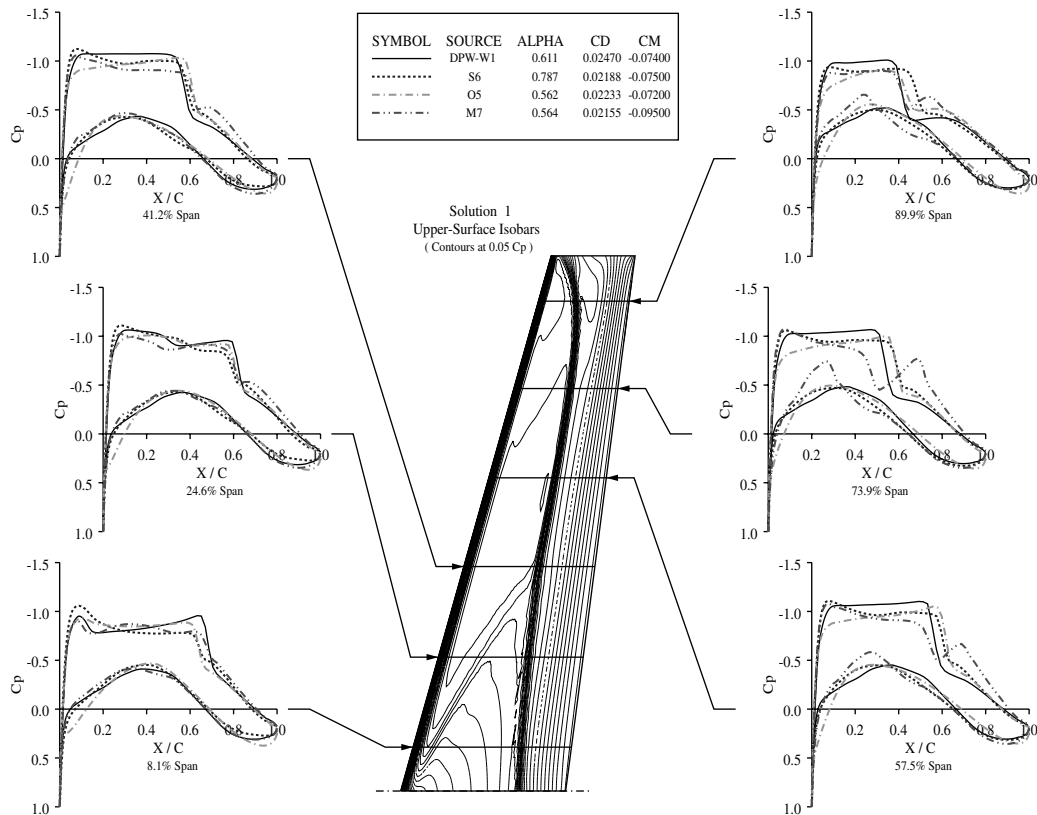


Fig. 20 Comparison of chordwise pressure distributions at $M = 0.78$, $C_L = 0.5$, and $Re = 5.0 \times 10^6$ for multipoint optimization cases with OVERFLOW computations.

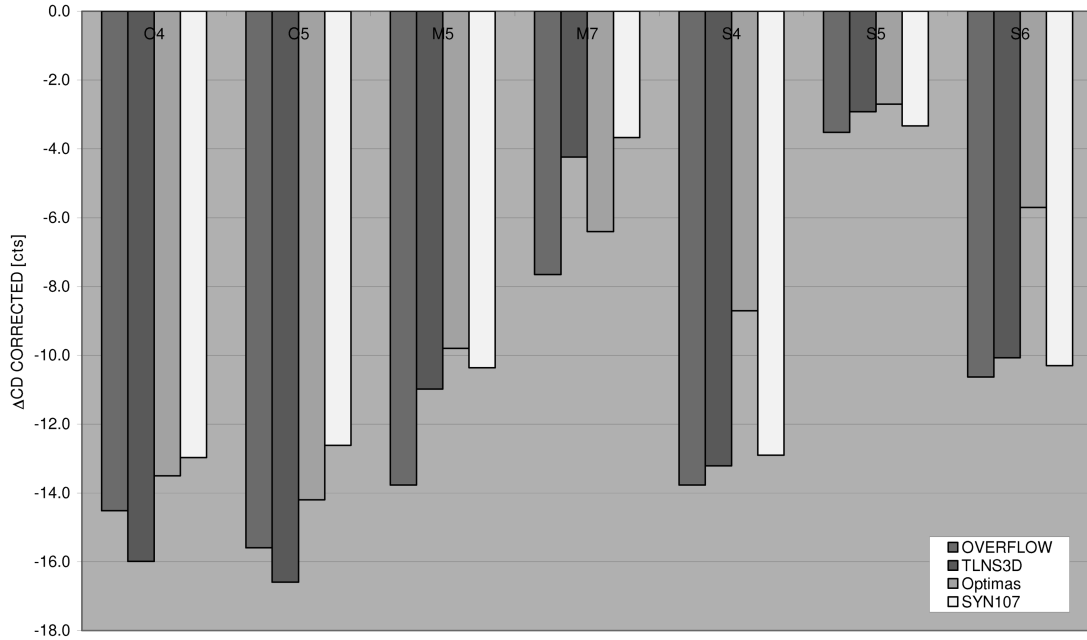


Fig. 21 Corrected drag-reduction values for the different optimal geometries at $M = 0.76$ and $C_L = 0.5$ for one-point optimizations of cases O4, M5, S4, and S5 and dual-point optimizations for cases O5, M7, and S6.

by the trim-drag penalty of 1 count per -0.01 in ΔC_M value, with no benefit incorporated if ΔC_M was positive. The corresponding bar charts with the corrected drag-reduction values are presented in Figs. 21 and 22 (for $M = 0.76$ and 0.78 , respectively).

Finally, to also estimate offdesign behavior of the optimized wings, we introduced the aggregate drag-reduction value, which is equal to the sum of ΔC_D achieved by an optimal geometry at $M = 0.76$ and 0.78 (corrected for trim-drag penalties). The corresponding bar charts with the corrected aggregate drag-reduction values are presented in Fig. 23.

The analysis of the presented data shows that, in general, the drag-reduction values estimated by different Navier–Stokes solvers correlated well for all of the considered optimal geometries. Specifically, it can be concluded that for all of the considered optimization tools, the reduction in drag due to optimization calculated by each associated CFD analysis code was confirmed by the other Navier–Stokes solvers with sufficient accuracy.

VII. Conclusions

A comparative study of CFD-based optimization techniques applied to the solution of a 3-D wing drag minimization problem was performed. Three independent optimization efforts were conducted concurrently, each without knowledge of the others' results. The baseline geometry of this pilot project is the public domain DPW-W1 wing (a test case for the 3rd AIAA Drag Prediction Workshop). The optimal geometries achieved by the aerodynamic design tools SYN107 (Intelligent Aerodynamics International), MDOPT (The Boeing Company), and OPTIMAS (Israel Aerospace Industries) were systematically cross-checked by each of CFD methods used in the optimization phase and by a fourth CFD method not used to develop any of the geometries. Lessons learned from this collaborative effort are documented. Based on this experience, detailed suggestions are provided to aid in the preparation of a possible future workshop on aerodynamic shape optimization.

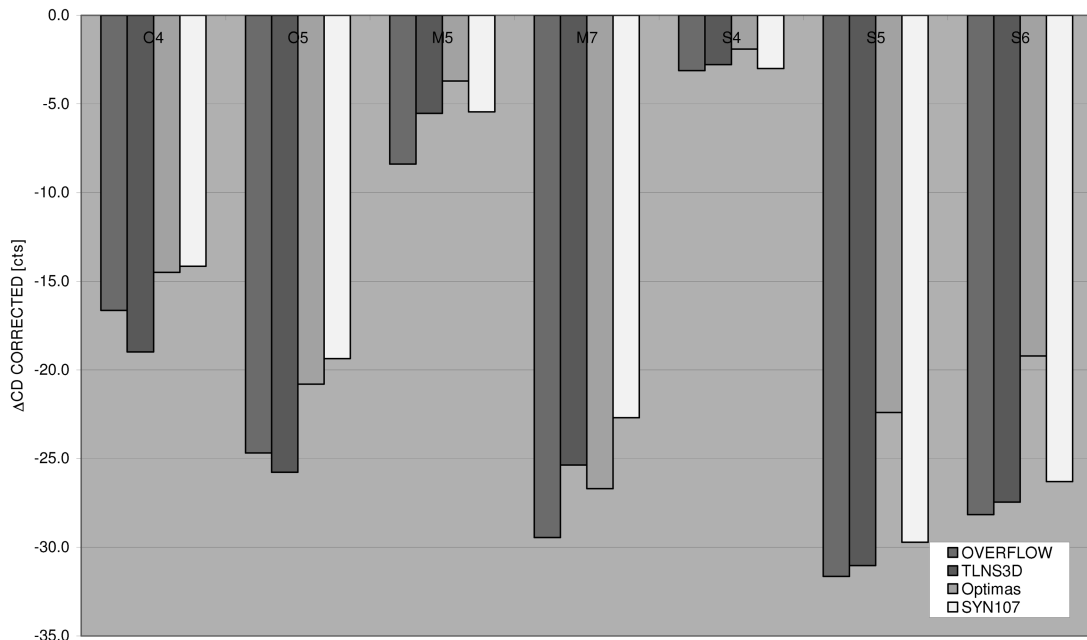


Fig. 22 Corrected drag-reduction values for the different optimal geometries at $M = 0.78$ and $C_L = 0.5$ for one-point optimizations of cases O4, M5, S4, and S5 and dual-point optimizations for cases O5, M7, and S6.

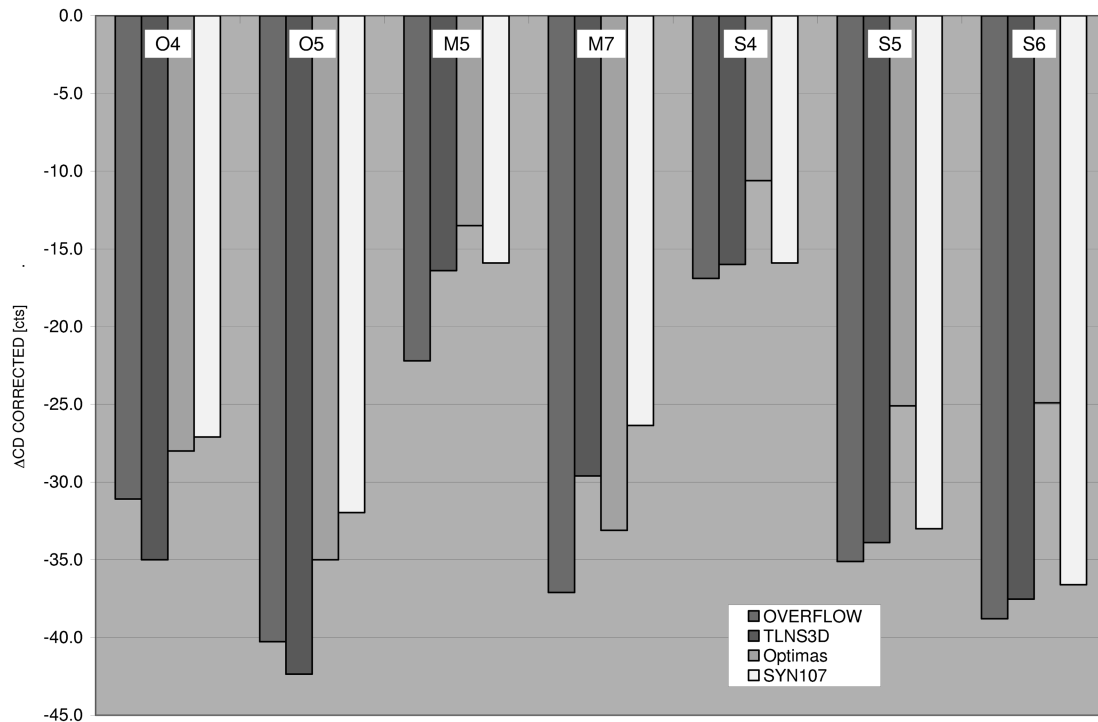


Fig. 23 Corrected aggregate drag-reduction values for the different optimal geometries at $C_L = 0.5$ for one-point optimizations of cases O4, M5, S4, and S5 and dual-point optimizations for cases O5, M7, and S6.

Acknowledgments

This work was supported by internal finding from The Boeing Company—Phantom Works, Israel Aerospace Industries, and Intelligent Aerodynamics, Inc. In particular, the authors thank Arnold Nathan, Adrian Rosenberg, and Stephane Seror of Israel Aerospace Industries and Tony Antani and Robb Gregg of The Boeing Company—Phantom Works for supporting this pilot project and encouraging the technical collaboration between organizations.

References

- [1] Jameson, A., Martinelli, L., and Vassberg, J., "Using Computational Fluid Dynamics for Aerodynamics—A Critical Assessment," International Council of the Aeronautical Sciences Paper 2002-1.10.1, Toronto, 2002.
- [2] Obayashi, S., Yamaguchi, Y., and Nakamura, T., "Multiobjective Genetic Algorithm for Multidisciplinary Design of Transonic Wing Planform," *Journal of Aircraft*, Vol. 34, No. 5, 1997, pp. 690–693. doi:10.2514/2.2231
- [3] Mohammadi, B., and Pironneau, O., *Applied Shape Optimization for Fluids*, Oxford Univ. Press, Oxford, 2001.
- [4] Vassberg, J., and Jameson, A., "Aerodynamic Shape Optimization of a Reno Race Plane," *International Journal of Vehicle Design*, Vol. 28, No. 4, 2002, pp. 318–338. doi:10.1504/IJVD.2002.001993
- [5] Epstein, B., and Peigin, S., "Robust Hybrid Approach to Multiobjective Constrained Optimization in Aerodynamics," *AIAA Journal*, Vol. 42, No. 8, 2004, pp. 1572–1581. doi:10.2514/1.992
- [6] Peigin, S., and Epstein, B., "Robust Handling of Non-Linear Constraints for GA Optimization of Aerodynamic Shapes," *International Journal for Numerical Methods in Fluids*, Vol. 45, No. 12, 2004, pp. 1339–1362. doi:10.1002/flid.747
- [7] Epstein, B., and Peigin, S., "Constrained Aerodynamic Optimization of Three-Dimensional Wings Driven by Navier–Stokes Computations," *AIAA Journal*, Vol. 43, No. 9, 2005, pp. 1946–1957. doi:10.2514/1.10308
- [8] Vassberg, J., and Jameson, A., "Aerodynamic Shape Optimization Part 1: Theoretical Background," *Introduction to Optimization and Multidisciplinary Design*, 2005–2006 VKI Lecture Series, von Karman Institute for Fluid Dynamics, Rhode-Saint-Genève, Belgium, 2006.
- [9] Vassberg, J., and Jameson, A., "Aerodynamic Shape Optimization Part 2: Sample Applications," *Introduction to Optimization and Multidisciplinary Design*, 2005–2006 VKI Lecture Series, von Karman Institute for Fluid Dynamics, Rhode-Saint-Genève, Belgium, 2006.
- [10] Selmin, V., "Multi-Point Aerodynamic Shape Optimization: The AEROSHAPE Project," *Proceedings of ECCOMAS 2000*, International Center for Numerical Methods in Engineering, Barcelona, 2000, pp. 138–139.
- [11] Wild, J., Brazilon, J., Amoignon, O., Quest, J., Moens, F., and Quagliarella, D., "Advanced High-Lift Design by Numerical Methods and Wind Tunnel Verification Within the European Project EUROLIFT II," AIAA Paper 2007-4300, 2007.
- [12] *4th AIAA CFD Drag Prediction Workshop* <http://aaac.larc.nasa.gov/tsab/cfdlarc/aiaa-dpw/Workshop3/workshop3.html> [retrieved 22 Apr. 2008].
- [13] Jameson, A., "Optimum Aerodynamic Design Using Control Theory," *CFD Review*, Wiley, Hoboken, NJ, 1995, pp. 495–528.
- [14] Jameson, A., "Aerodynamic Design via Control Theory," *Journal of Scientific Computing*, Vol. 3, No. 3, 1988, pp. 233–260. doi:10.1007/BF01061285
- [15] Jameson, A., "Computational Aerodynamics for Aircraft Design," *Science*, Vol. 245, No. 28, 1989, pp. 361–371. doi:10.1126/science.245.4916.361
- [16] Jameson, A., "Optimum Aerodynamic Design Using CFD and Control Theory," 12th AIAA Computational Fluid Dynamics Conference, AIAA Paper 1995-1729, 1995.
- [17] Jameson, A., Pierce, N. A., and Martinelli, L., "Optimum Aerodynamic Design Using the Navier–Stokes Equations," *Theoretical and Computational Fluid Dynamics*, Vol. 10, No. 1, 1998, pp. 213–237. doi:10.1007/s001620050060
- [18] Jameson, A., and Martinelli, L., "Aerodynamic Shape Optimization Techniques Based on Control Theory," *Lecture Notes in Mathematics*, Vol. 1739, May 2000, pp. 151–221.
- [19] Jameson, A., and Vassberg, J., "Studies of Alternative Numerical Optimization Methods Applied to the Brachistotrone Problem," *Computational Fluid Dynamics Journal*, Vol. 9, No. 3, 2000, pp. 281–296.
- [20] Jameson, A., and Vassberg, J., "Computational Fluid Dynamics for Aerodynamic Design: Its Current and Future Impact," AIAA Paper 2001-0538, 2001.
- [21] Leoviriyakit, K., Kim, S., and Jameson, A., "Aero-Structural Wing Planform Optimization Using the Navier–Stokes Equations," 10th AIAA/ISSMO Multidisciplinary Analysis and Optimization Conference, Albany, NY, AIAA Paper 2004-4479, 2004.
- [22] LeDoux, S. T., Herling, W. W., Fatta, J., and Ratcliff, R. R., "Multidisciplinary Design Optimization System Using Higher Order

- Analysis Code,” 10th AIAA/ISSMO Multidisciplinary Analysis and Optimization Conference, Albany, NY, AIAA Paper 2004-4567, 2004.
- [23] Audet, C., Dennis, J., Moore, D., Booker, A., and Frank, P., “Surrogate-Model-Based Method for Constrained Optimization,” AIAA Multi-Disciplinary Optimization Conference, AIAA Paper 2000-4891, 2000.
- [24] Ratcliff, R. R., LeDoux, S. T., and Herling, W. W., “Modern CORBA-Based Approach to Ad Hoc Distributed Process Orchestrations Applied to MDO,” Infotech@Aerospace, Arlington, VA, AIAA Paper 2005-7143, 2005.
- [25] Michalewicz, Z., *Genetic Algorithms + Data Structures = Evolution Programs*, Springer-Verlag, New York, 1996.
- [26] Peigin, S., and Epstein, B., “Robust Drag Minimization of Aerodynamic Wings in Engineering Environment,” *Journal of Aircraft*, Vol. 43, No. 4, 2006, pp. 1195–1204. doi:10.2514/1.18634
- [27] Vatsa, V. N., and Hammond, D. P., “Viscous Flow Computations for Complex Geometries on Parallel Computers,” *4th NASA Symposium on Large-Scale Analysis and Design on High-Performance Computers and Workstations*, July 1997.
- [28] Epstein, B., Rubin, T., and Seror, S., “Accurate Multiblock Navier–Stokes Solver for Complex Aerodynamic Configurations,” *AIAA Journal*, Vol. 41, No. 4, 2003, pp. 582–594. doi:10.2514/2.2012
- [29] Vassberg, J. C., DeHaan, M. A., and Sclafani, A. J., “Grid Generation Requirements for Accurate Drag Predictions Based on OVERFLOW Calculations,” 16th AIAA Computational Fluid Dynamics Conference, Orlando, FL, AIAA Paper 2003-4124, 2003.
- [30] Jameson, A., “Multigrid Algorithms for Compressible Flow Calculations,” *Lecture Notes in Mathematics*, Vol. 1228, edited by W. Hackbusch and U. Trottenberg, Springer-Verlag, Berlin, June 2006, pp. 166–201
- [31] Spalart, P. R., and Allmaras, S. R., “A One-Equation Turbulence Model for Aerodynamic Flows,” AIAA Paper 1992-0439, 1992.
- [32] Chan, W. M., and Steger, J. L., “Enhancements of a Three-Dimensional Hyperbolic Grid Generation Scheme,” *Applied Mathematics and Computation*, Vol. 51, No. 2, 1992, pp. 181–205. doi:10.1016/0096-3003(92)90073-A
- [33] Jones, W. T., and Samareh-Abolhassani, J., “Grid Generation System for Multi-Disciplinary Design Optimization,” 12th AIAA Computational Fluid Dynamics Conference, San Diego, CA, AIAA Paper 1995-1689, 1995.
- [34] Seror, S., Rubin, T., Peigin, S., and Epstein, B., “Implementation and Validation of the Spalart-Allmaras Turbulence Model for a Parallel CFD Code,” *Journal of Aircraft*, Vol. 42, No. 1, 2005, pp. 179–188. doi:10.2514/1.4009
- [35] Baldwin, B. S., and Lomax, H., “Thin Layer Approximation and Algebraic Model for Separated Turbulent Flows,” AIAA Paper 1978-0257, 1978.
- [36] Peigin, S., Epstein, B., Rubin, T., and Seror, S., “Parallel Large Scale High Accuracy Navier–Stokes Computations on Distributed Memory Clusters,” *Journal of Supercomputing*, Vol. 27, No. 1, 2004, pp. 49–68. doi:10.1023/A:1026246805774
- [37] Peigin, S., and Epstein, B., “Embedded Parallelization Approach for Optimization in Aerodynamic Design,” *Journal of Supercomputing*, Vol. 29, No. 3, 2004, pp. 243–263. doi:10.1023/B:SUPE.0000032780.68664.1b
- [38] Buning, P. G., Jespersen, D. C., Pulliam, T. H., Chan, W. M., Slotnick, J. P., Krist, S. E., and Renze, K. J., “OVERFLOW User’s Manual, Ver. 1.81,” NASA Langley Research Center, Hampton, VA, 1999.
- [39] Sclafani, A. J., Vassberg, J. C., Harrison, N. A., DeHaan, M. A., Rumsey, C. L., Rivers, S. M., and Morrison, J. H., “Drag Predictions for the DLR-F6 Wing/Body and DPW Wings Using CFL3-D and OVERFLOW on an Overset Mesh,” 45th AIAA Aerospace Sciences Meeting and Exhibit, Reno, NV, AIAA Paper 2007-0256, 2007.